Bulk Metallic Glasses Deform via Slip Avalanches

James Antonaglia,[1] Wendelin J. Wright,[2,3] Xiaojun Gu,[2] Rachel R. Byer,[4] Todd C. Hufnagel,[5] Michael LeBlanc,[1] Jonathan T. Uhl,[*] and Karin A. Dahmen[1,†]

[1]*Department of Physics and Institute of Condensed Matter Theory, University of Illinois at Urbana Champaign, 1110 West Green Street, Urbana, Illinois 61801, USA*

[2]*Department of Mechanical Engineering, One Dent Drive, Bucknell University, Lewisburg, Pennsylvania 17837, USA*

[3]*Department of Chemical Engineering, One Dent Drive, Bucknell University, Lewisburg, Pennsylvania 17837, USA*

[4]*Department of Physics and Astronomy, One Dent Drive, Bucknell University, Lewisburg, Pennsylvania 17837, USA*

[5]*Department of Materials Science and Engineering, Johns Hopkins University, 3400 North Charles Street, Baltimore, Maryland 21218, USA*

(Received 21 December 2013; published 14 April 2014)

For the first time in metallic glasses, we extract both the exponents and scaling functions that describe the nature, statistics, and dynamics of slip events during slow deformation, according to a simple mean field model. We model the slips as avalanches of rearrangements of atoms in coupled shear transformation zones (STZs). Using high temporal resolution measurements, we find the predicted, different statistics and dynamics for small and large slips thereby excluding self-organized criticality. The agreement between model and data across numerous independent measures provides evidence for slip avalanches of STZs as the elementary mechanism of inhomogeneous deformation in metallic glasses.

DOI: 10.1103/PhysRevLett.112.155501 PACS numbers: 62.20.F−, 81.70.Bt

We show here that slowly compressed metallic glasses deform plastically via slip avalanches of elastically coupled weak spots. The weak spots are shear transformation zones (STZs), which are collective rearrangements of 10–100 atoms [1].

During high temperature deformation of metallic glasses (close to the glass transition), STZs operate independently and the material flows homogeneously, in agreement with STZ theory predictions over several orders of magnitude of stress and strain rate [1,2]. At lower temperatures metallic glasses deform inhomogeneously via intermittent slips on narrow shear bands [3]. At low strain rates, these slip events are manifested as sudden stress drops, called serrated flow. Analytical [4,5] and computational investigations [6–8] suggest STZ operation, but experimental support has been challenging because slip events are both fast (with millisecond durations) and highly localized (with thicknesses <1 μm) [3]. Here we report experimental results on the stress-drop dynamics and statistics, finding excellent agreement with analytic model predictions for the slip avalanche statistics of coupled weak spots or STZs.

Many other materials—including crystals and densely packed granular solids—exhibit sudden slips during inelastic deformation. Although the mechanisms of deformation differ, the statistics and dynamics of the slip events are described by the same simple mean-field model of plastic deformation [9,10]. The model assumes that weak spots slip and then restick whenever the local shear stress exceeds a random local slip threshold. Weak spots in crystals are dislocations, while in a metallic glass they are STZs. Through elastic interactions a slipping weak spot can trigger others to slip, creating a slip avalanche. In crystals the slip can locally strengthen the material, while in metallic glasses it weakens it (through dilatation from STZ operation). For weakening materials (such as metallic glasses) the model assumes temporal threshold weakening for slipping sites that lasts until the slip avalanche is completed. For these materials, the model predicts two types of slip avalanches: (1) small slip avalanches with a power law size distribution and self-similar dynamics, and (2) less frequent but almost regularly recurring large slip avalanches with cracklike scaling behavior [9,10]. The model predicts both the statistics and the dynamics of the slip avalanches. Its agreement with experimental observations provides strong evidence that shear banding in metallic glasses arises from the collective slips of coupled STZs.

To test the model we conducted uniaxial compression testing of metallic glass specimens in a high-stiffness, precisely aligned loading train with a fast-response load cell and high-rate data acquisition [Fig. 1(a) and the Supplemental Material [11]]. During compression the specimen deforms elastically until a shear band or slip event initiates. This causes the displacement rate to temporarily exceed the displacement rate imposed on the specimen, resulting in a stress drop [Fig. 1(b)]. The size of the stress drop is proportional to the slip size. Subsequently the stress increases until initiation of another slip event. We measure the stress drops in our metallic glass with high temporal resolution to resolve the dynamics of the slip events. This enables us to extract a wide range of predicted scaling exponents and scaling functions that uniquely identify the underlying slip statistics and dynamics.

We briefly summarize some of the model predictions for the stress-drop statistics in weakening materials [9,10] and the agreement with the experimental data. The complementary cumulative size distribution $C(S)$, (i.e., the fraction

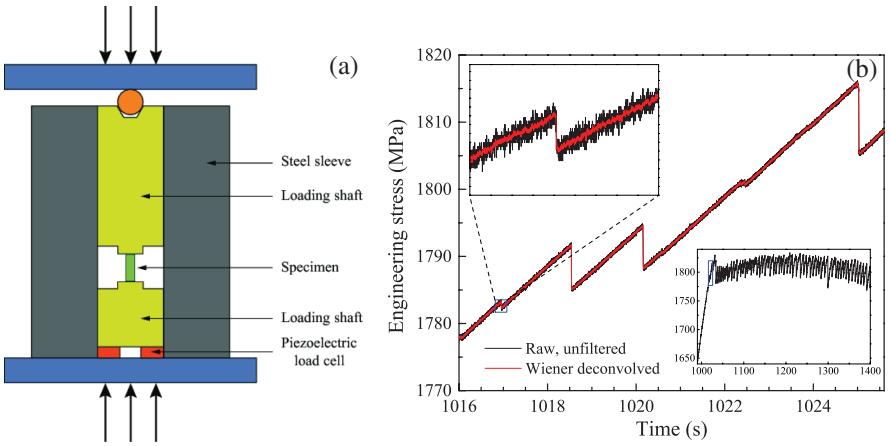

FIG. 1 (color online). Experimental setup and stress drops. (a) Schematic diagram of experimental setup. Two tungsten carbide platens that are constrained by a steel sleeve compress the metallic glass specimen, see Ref. [15] for details. (b) Lower-right inset: applied stress versus time. Main figure: magnification of data in the small window in the lower-right inset. Slip avalanches are manifest as sudden drops in applied stress. Upper-left inset is further magnification, showing one stress drop. Black curves indicate raw, unfiltered stress time series, and gray (red) curves indicate the time series after Wiener deconvolution.

of stress drops larger than size S) scales as $C(S) \sim S^{-1/2}$ for the (small) avalanches spanning the power law scaling regime of sizes $S_{\min} < S < S_{\max}$ [Fig. 2(a)]. $S_{\min}$ is the experimental noise threshold [visible in Fig. 2(c)]. $S_{\max}$ is related to the low-frequency roll off $\omega_{\min}$ of the power spectrum $P(\omega)$, which is the absolute square of the Fourier transform of the stress-drop rate time series [see Fig. 2(d)]. The model predicts $P(\omega) \sim 1/\omega^2$ for frequency $\omega \gg \omega_{\min}$, and $P(\omega) \to$ constant for $\omega \ll \omega_{\min}$. Furthermore $\omega_{\min} \sim 1/T_{\max} \sim 1/(S_{\max})^{1/2}$, with upper duration limit $T_{\max}$ and upper size limit $S_{\max}$ of the scaling regime in Figs. 2(a)–2(c). Figures 2(a)–2(d) show agreement of experiments with predictions for $C(S)$, the average avalanche durations T at size S, the maximum stress-drop rate at size S, and $P(\omega)$ (before and after Wiener filtering, see the Supplemental Material [11]) [9,10,16,17]. In each case the

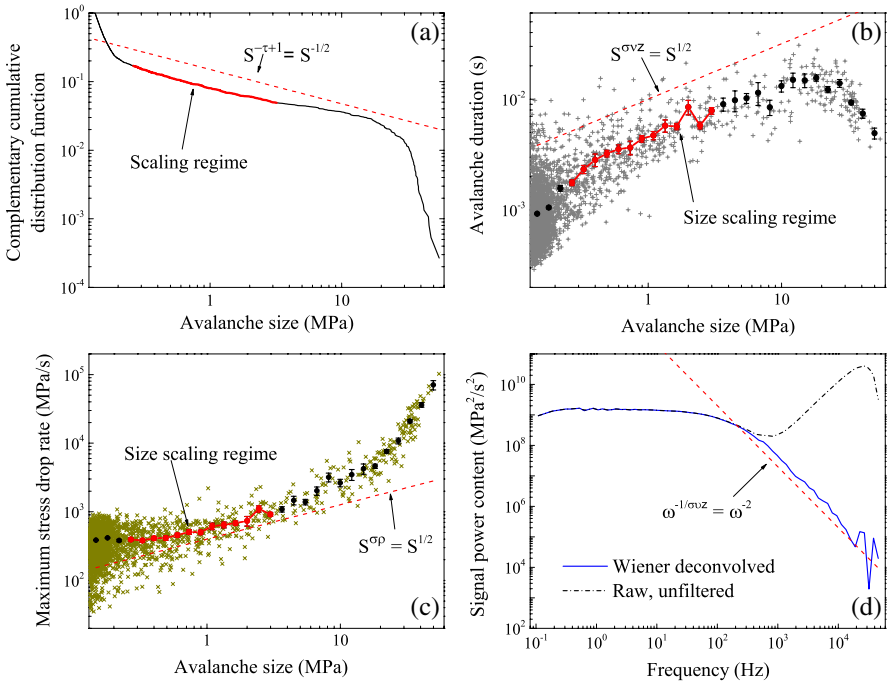

FIG. 2 (color online). Experimental avalanche statistics. Gray (red) dashed lines indicate model predictions [9,10,16,17]. (a) Distribution of stress-drop sizes (3744 avalanches). The scaling-regime [gray (red)] extends from 2.6×10^5 to 3.3×10^6 Pa, limited by high frequency noise (left) and large cracklike stress drops (right). (b) Avalanche duration T versus size S. (c) Maximum stress-drop rates versus stress-drop size. (b),(c) One cross per avalanche. Black dots indicate average duration (b) or average maximum stress-drop rate (c) in one of 30 size bins. Error bars indicate 68% confidence interval. (d) Power spectrum of stress-drop rate time series, before and after Wiener filtering.

power law exponents of the observed serration statistics agree with the model predictions. We also observe agreement with eight other statistical measures, including predicted scaling functions, as discussed in Figs. 3 and 4 and the Supplemental Material [11]. Although some power law distributions of slip sizes in metallic glasses have been studied [18], no experimental data have previously been obtained for the slip statistics and the dynamics, and no model predictions have previously been shown to agree with the many different statistical measures of Figs. 2–4 and the Supplemental Material [11] that include not only multiple predicted scaling exponents but also predicted scaling functions.

We use high temporal resolution measurements to test the predicted dynamics of individual slip events, which are sensitive to key assumptions of the model. Adding inertial or weakening effects [21–24] or a delayed damping term [25] to the model changes its predictions for avalanche dynamics [24–26] even though they may (or may not) affect the critical exponents of the slip statistics (Fig. 2).

The model predicts the temporal profiles of the small avalanches, i.e., the stress-drop rate as a function of time averaged over all slips of similar duration T. Figures 3(a) and 3(b) compare the experimental profiles, scaled by their duration T, to the model predictions. The measured profiles look symmetric, as shown more clearly in Figs. 3(c), 3(d), and 4(a), in remarkable agreement with the simple mean field model that neglects both inertia and delay effects. As shown in Fig. 4(b) models with inertial-weakening effects predict asymmetric profiles that are tilted to the right [25,26], while models with delayed damping effects predict profiles tilted to the left (as observed for Barkhausen noise and large earthquakes) [25,27–29]. In the inset to Fig. 4(c) we show average avalanche profiles for four different avalanche sizes S (rather than durations T). The avalanche profiles collapse onto the predicted symmetric scaling function when both axes are rescaled by the predicted factor $S^{-1/2}$.

The comparison of scaling functions in Figs. 3 and 4 is a much more stringent test of the model than any traditionally used discrete set of power-law exponents. The extensive tests of slip statistics (Fig. 2 and the Supplemental Material [11]) and slip dynamics (Figs. 3 and 4) thus confirm that inhomogeneous deformation of metallic glasses proceeds via slip avalanches of STZs. Furthermore, the data are consistent with the model prediction that inhomogeneous deformation of metallic glasses is an ordinary (tuned) critical phenomenon with a limited scaling regime, as opposed to a self-organized critical phenomenon [18] (which would require self-similarity to apply to all avalanches, small and large). The results indicate that inertial and delay effects are negligible for the slip statistics and dynamics of the small avalanches.

The two types of avalanches (small and large) predicted by the model and observed in the experiments correspond to different modes of shear propagation (Fig. S3 in the Supplemental Material [11]). Small slips result from progressive deformation, i.e., a propagating shear front with little or no slip occurring behind the front. Large slips are akin to a mode II crack with uniform sliding along the entire shear plane [9,10]. In the experiments, the small slips occur when a shear band nucleates at a stress concentration

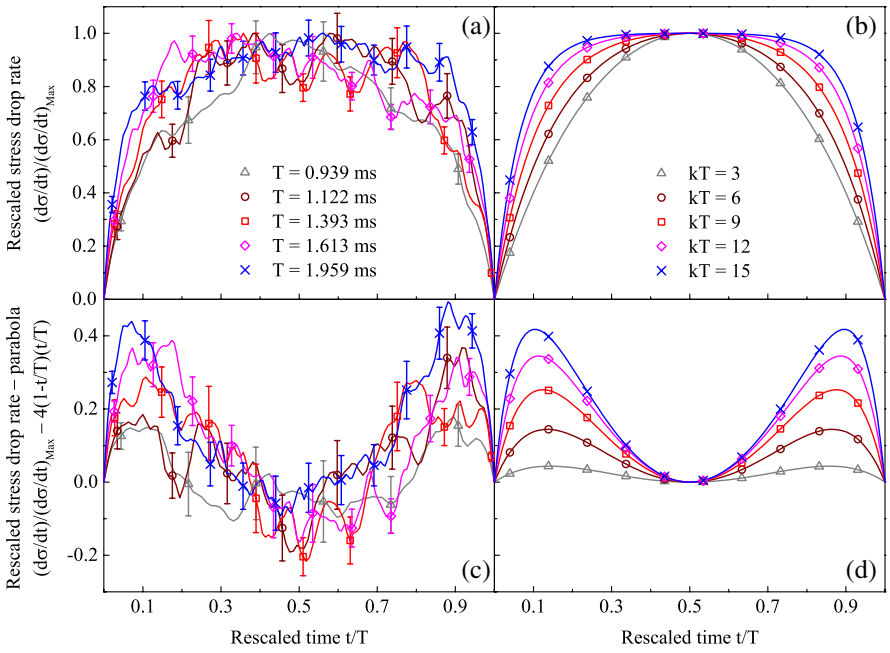

FIG. 3 (color online). Temporal avalanche profiles. (a) Average stress-drop rate divided (normalized) by its maximum rate. Profiles are averaged over avalanches from small bins of their durations. Error bars indicate 68% confidence intervals in each bin. (b) Predicted average profiles from mean field theory. For increasing avalanche duration T, profiles become flatter, reflecting finite size effects, parametrized by k [19]. (c),(d) Difference between the normalized stress-drop rate and the parabolic form predicted for small avalanches. Larger avalanches deviate more from a parabola, consistent with the model prediction [19]. Note the clear symmetry of the profiles.

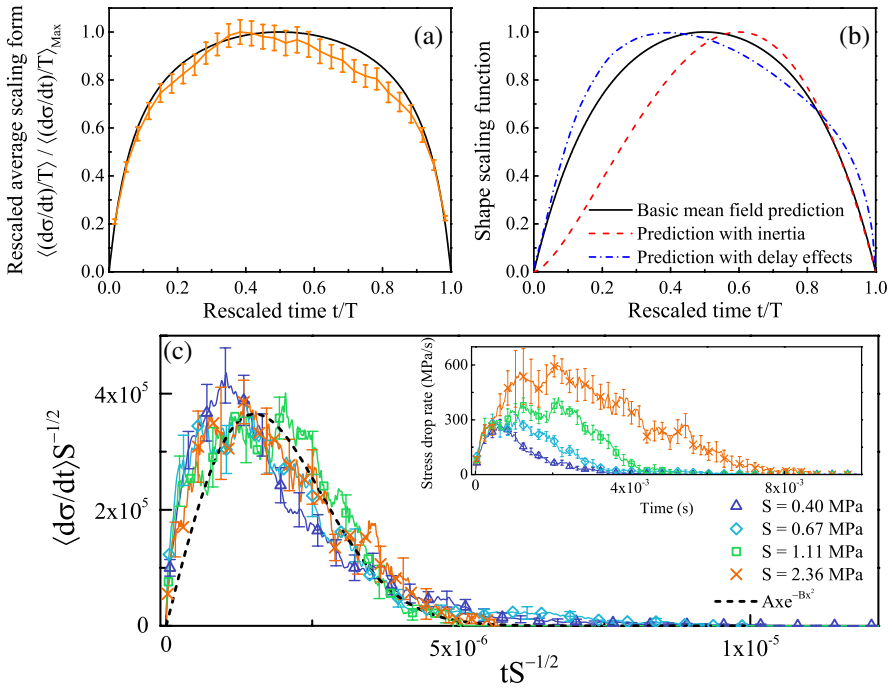

FIG. 4. (color online). Average avalanche profiles. (a) Stress-drop rate profiles divided by duration T averaged over all small avalanches in the scaling regime. Agreement with the model prediction for fitting parameter $k = 1880 \pm 80\ \mathrm{s}^{-1}$ (see the Supplemental Material [11]). (b) Model predictions for average avalanche profiles for different model assumptions [19,25–27]. (c) Inset shows unscaled average stress-drop rate profiles for different stress-drop sizes S, collapsed in the main figure (scaling both axes by a factor of $S^{-1/2}$). Agreement of collapse with predicted collapse scaling function (black dotted line, for nonuniversal values of the constants $A = 3.98 \times 10^{11}$ and $B = 2.18 \times 10^{11}$; see the Supplemental Material [11]) [20,29].

(such as the specimen-platen interface or an internal pore) and propagates as a front away from the concentration into a region of lower stress. The reduced driving stress causes the shear band to arrest after only a limited amount of slip and a correspondingly small stress drop. The large stress drops occur when a shear band manages to span the specimen, allowing continued simultaneous shear deformation on a plane at (approximately) 45° to the loading axis [30,31]. Slipping stops when the shear stress drops below a critical stress at which point the shear band arrests. This agrees with the model prediction of cracklike scaling behavior of the large slip avalanches [9,10].

As assumed in the model, structural disorder and the presence of defects cause the critical stresses at which slips initiate or stop to vary throughout the specimen. For both large and small avalanches, dilatation during STZ operation leads to a decrease in viscosity of the material in the shear band. This weakening is the key tuning parameter of the model [9,10] that determines the size of the scaling regime for the small avalanches.

The extent of the power-law scaling regime we observe is limited by the occurrence of large, cracklike slip events. Much larger power-law scaling regimes can be observed in the absence of such events (as, for example, in certain porous materials [32–34]). Furthermore, although it is possible that merging of avalanches might change the interpretation of our data, theory and simulations suggest that merged avalanches would lead to larger deviations from the mean-field theory than we observe at the current time resolution [35,36]. We therefore expect the effects of merged avalanches to be small, although measurements with higher spatial and temporal resolution are required to resolve this question definitively.

In summary, high temporal-resolution experiments on the slow compression of metallic glasses for the first time simultaneously measure slip statistics and slip dynamics. The results agree with predictions of a simple mean field model [9,10]. This agreement implies that inhomogeneous deformation in bulk metallic glasses proceeds via slip avalanches of weak spots, as assumed by the model, and provides compelling experimental evidence for the importance of shear transformation zones in the initiation and operation of shear bands. The prediction and observation of two types of avalanches (small ones marked by scaling behavior and large ones above the scaling regime) is associated with two modes of shear band operation. Small slip events correspond to nucleation and propagation of shear fronts. Some small slips grow sufficiently large to exceed a critical stress and transition into large slip events with cracklike sliding across a mature shear band. The high information content contained in the serration statistics and the dynamic avalanche profiles allow discrimination among competing models [19,37], suggesting that similar experiments will provide new insights into deformation mechanisms of other materials.

Materials and methods.—Three-millimeter-diameter rods of $Zr_{45}Hf_{12}Nb_5Cu_{15.4}Ni_{12.6}Al_{10}$ were prepared using arc melting and suction casting and verified to be amorphous with x-ray diffraction. Rectangular parallelepiped specimens 6 mm long with a cross-sectional area of 2 by 1.5 mm with tight dimensional tolerances (reported previously in Ref. [15]) were machined from the cast ingots. Quasistatic uniaxial compression tests were performed at a constant displacement rate and a nominal strain rate of 10^{-4} s^{-1} using a screw-driven Instron 5584 in a high-stiffness, precisely aligned load train as shown in Fig. 1(a). The stress data were acquired using a 60 kN Kistler piezoelectric load cell with a 180 kHz low-pass filter. The data were recorded using a Hi-Techniques Synergy P system at a rate of 100 kHz with a 40 kHz low-pass filter. The displacement data were acquired using an Epsilon Tech 3442 extensometer. Metallic glasses fail catastrophically under uniaxial compression with fracture propagating at speeds on the order of 170 m/s or faster [30]. For specimens of this size, the fracture event occurs over an elapsed time that is less than 12.5 μs. High-speed imaging confirms that the electronics of the system are unable to accurately track this rapid fracture event due to the presence of the low-pass filters. The fracture event therefore functions as a unit impulse to the system, and the corresponding stress versus time data are used as the unit impulse response for the purposes of Wiener filtering (see the Supplemental Material [11]). The durations of the slip events range from 0.73 to 21.1 ms, while the applied stress is recorded every 10 μs; therefore, we record, on average, several hundred data points during each stress drop, allowing us to extract information about both the statistics of the stress drops as well as the dynamics of individual slip events.

We thank Braden Brinkman, Sean Clarke, Nir Friedman, and Matthew Wraith for helpful conversations. We acknowledge support from NSF Grant No. DMR-1042734 (W. J. W.), NSF Grant No. DMR-1107838 (T. C. H.), NSF Grants No. DMR-1005209 and No. NSF DMS-1069224 (K. A. D.), and MGA. J. A. and W. J. W. contributed equally to this work.

*Retired.
†Corresponding author.
dahmen@illinois.edu

[1] C. A. Schuh, T. C. Hufnagel, and U. Ramamurty, Acta Mater. **55**, 4067 (2007).
[2] J. Lu, G. Ravichandran, and W. L. Johnson, Acta Mater. **51**, 3429 (2003).
[3] A. L. Greer, Y. Q. Cheng, and E. Ma, Mater. Sci. Eng. R **74**, 71 (2013).
[4] A. S. Argon, Acta Metall. **27**, 47 (1979).
[5] P. S. Steif, F. Spaepen, and J. W. Hutchinson, Acta Metall. **30**, 447 (1982).
[6] E. R. Homer and C. A. Schuh, Acta Mater. **57**, 2823 (2009).
[7] M. L. Falk and J. S. Langer, Annu. Rev. Condens. Matter Phys. **2**, 353 (2011).
[8] M. J. Demkowicz and A. S. Argon, Phys. Rev. B **72**, 245206 (2005).
[9] K. A. Dahmen, Y. Ben-Zion, and J. T. Uhl, Nat. Phys. **7**, 554 (2011).
[10] K. A. Dahmen, Y. Ben-Zion, and J. T. Uhl, Phys. Rev. Lett. **102**, 175501 (2009).
[11] See Supplemental Material, which includes Refs. [12–14], at http://link.aps.org/supplemental/10.1103/PhysRevLett.112.155501 for detailed information on the avalanche analysis, the experimental observations, and the list of the twelve observations on the avalanche statistics and their comparison to model predictions.
[12] N. Gershenfeld, *The Nature of Mathematical Modeling* (Cambridge University Press, Cambridge, England, 1999).
[13] J. P. Sethna, K. A. Dahmen, and C. R. Myers, Nature (London) **410**, 242 (2001).
[14] H. J. Leamy, H. S. Chen, and T. T. Wang, Metall. Trans. **3**, 699 (1972).
[15] W. J. Wright, M. W. Samale, T. C. Hufnagel, M. M. LeBlanc, and J. N. Florando, Acta Mater. **57**, 4639 (2009).
[16] M. LeBlanc, L. Angheluta, K. A. Dahmen, and N. Goldenfeld, Phys. Rev. Lett. **109**, 105702 (2012).
[17] M. LeBlanc, L. Angheluta, K. Dahmen, and N. Goldenfeld, Phys. Rev. E **87**, 022126 (2013).
[18] J. L. Ren, C. Chen, G. Wang, N. Mattern, and J. Eckert, AIP Adv. **1**, 032158 (2011).
[19] S. Papanikolaou, F. Bohn, R. L. Sommer, G. Durin, S. Zapperi, and J. P. Sethna, Nat. Phys. **7**, 316 (2011).
[20] D. S. Fisher, Phys. Rep. **301**, 113 (1998).
[21] S. Ramanathan and D. S. Fisher, Phys. Rev. B **58**, 6026 (1998).
[22] J. M. Schwarz and D. S. Fisher, Phys. Rev. Lett. **87**, 096107 (2001).
[23] J. M. Schwarz and D. S. Fisher, Phys. Rev. E **67**, 021603 (2003).
[24] D. S. Fisher, K. Dahmen, S. Ramanathan, and Y. Ben-Zion, Phys. Rev. Lett. **78**, 4885 (1997).
[25] S. Zapperi, C. Castellano, F. Colaiori, and G. Durin, Nat. Phys. **1**, 46 (2005).
[26] A. Baldassarri, F. Colaiori, and C. Castellano, Phys. Rev. Lett. **90**, 060601 (2003).
[27] K. A. Dahmen, Nat. Phys. **1**, 13 (2005).
[28] A. P. Mehta, A. C. Mills, K. A. Dahmen, and J. P. Sethna, Phys. Rev. E **65**, 046139 (2002).
[29] A. P. Mehta, K. A. Dahmen, and Y. Ben-Zion, Phys. Rev. E **73**, 056104 (2006).
[30] W. J. Wright, R. R. Byer, and X. J. Gu, Appl. Phys. Lett. **102**, 241920 (2013).
[31] S. X. Song, X.-L. Wang, and T. G. Nieh, Scr. Mater. **62**, 847 (2010).
[32] J. Baró, A. Corral, X. Illa, A. Planes, E. K. H. Salje, W. Schranz, D. E. Soto-Parra, and E. Vives, Phys. Rev. Lett. **110**, 088702 (2013).
[33] E. K. H. Salje, G. I. Lampronti, D. E. Soto-Parra, J. Baró, A. Planes, and E. Vives, Am. Mineral. **98**, 609 (2013).
[34] E. K. H. Salje, D. E. Soto-Parra, A. Planes, E. Vives, M. Reinecker, and W. Schranz, Philos. Mag. Lett. **91**, 554 (2011).
[35] R. A. White and K. A. Dahmen, Phys. Rev. Lett. **91**, 085702 (2003).
[36] M. LeBlanc and K. A. Dahmen (unpublished).
[37] K. M. Salerno, C. E. Maloney, and M. O. Robbins, Phys. Rev. Lett. **109**, 105703 (2012).